ELSEVIER

Journal of Power Sources 112 (2002) 137–152

JOURNAL OF POWER SOURCES

www.elsevier.com/locate/jpowsour

A two-dimensional steady-state model for phosphoric acid fuel cells (PAFC)

Suman Roy Choudhury[a], M.B. Deshmukh[a], R. Rengaswamy[b,*]

[a]*Naval Materials Research Laboratory, Ambernath, Maharashtra, India*

[b]*Department of Chemical Engineering, Clarkson University, Potsdam, NY 13699-5705, USA*

Received 22 May 2002; accepted 13 June 2002

Abstract

A two-dimensional steady-state model for a phosphoric acid fuel cell (PAFC) is developed. While most of the published literature deals with one-dimensional models for PAFC, a two-dimensional model is necessitated in cases where the oxygen concentration changes substantially in the flow direction due to depletion of oxygen and back diffusion of product water. The proposed modeling strategy was validated by: (i) testing in one-dimensional mode for verification of the basic parameters through a micro setup known as ''unit cell'', and (ii) evaluation of the two-dimensional model through an experimental setup of a PAFC stack with four cells. Further, the utility of the model in design and humidity management, and parametric sensitivity studies are presented.

Keywords: Phosphoric acid fuel cells (PAFCs); Two-dimensional model; Mathematical modeling

1. Introduction

The need for highly efficient and low emission energy conversion devices has attracted attention towards fuel cells world over. A fuel cell is an electrochemical device which converts chemical energy to electrical energy directly. Out of several families of fuel cells, hydrogen–oxygen fuel cells are an important class of fuel cells for which the technology is mature enough for practical usage. Fuel cells have been used in the past in space applications. Other possible applications include small to medium sized stationary power generation plants, vehicle propulsion, various types of power sources for military use and so on. Of the hydrogen–oxygen fuel cell systems, the most mature is phosphoric acid fuel cell (PAFC). It operates at 150–190 °C and pressures ranging from ambient to 5 atm. PAFC systems primarily use Pt as a catalyst, both for hydrogen and oxygen electrodes. Operating temperature range of PAFC allows it to take up hydrogen directly from hydrogen sources like reformer gases. CO (less than 1%) present in the reformer gases are not adsorbed on Pt sites owing to the high operating temperature. The other components used in PAFC are mainly made of graphite and carbon. All these make PAFC a versatile member of the hydrogen–oxygen fuel cell family.

As a part of the PAFC research program in Naval Materials Research Laboratory (NMRL), India, modeling of PAFC stacks of various capacities and configurations are being developed. Numerous parameters like electrode characteristics, gas flow fields, acid concentration, temperature, inlet partial pressures of the reactants and so on have significant effect on the performance of a PAFC stack. It is, therefore, difficult to analyze the effect of each parameter through experimentation in order to design PAFC components optimally. A comprehensive model allows in depth study of the system at various operating conditions with several possible combinations of the component parameters. Another advantage of a good representative model is easy development of diagnostic tools [1] for determining possible malfunctions inside large sized, higher capacity stacks. Stable operation of medium to high capacity PAFC stacks require balancing of several operational parameters like flow rates, humidity and temperature. The output electrical potential of a PAFC stack is a function of its energy conversion efficiency. Thus, under variable load, it is important to maintain the potential at the maximum possible value in order to maximize energy conversion efficiency. In this paper, we develop a two-dimensional steady-state model for PAFC to study and understand the

* Corresponding author. Tel.: +1-315-268-4423; fax: +1-315-268-6654.
E-mail address: raghu@clarkson.edu (R. Rengaswamy).

0378-7753/02/$ – see front matter © 2002 Published by Elsevier Science B.V.
PII: S0378-7753(02)00369-5

Nomenclature

a_a	effective area of catalyst site per unit volume of agglomerate (cm^2 cm^{-3})
a_c	groove cross-section (cm^2)
A^*	cross-section area of an agglomerate in YZ-plane (cm^2)
b	normal Tafel slope (V per decade)
c_{os}	concentration of oxygen on surface of agglomerate (gmol cm^{-3})
c_{1a}	concentration of oxygen inside agglomerate (gmol cm^{-3})
$c_{H_3PO_4}$	phosphoric acid concentration in percent ortho phosphoric acid equivalent
D_{agg}	effective diffusivity inside agglomerate for oxygen (cm^2 s^{-1})
D_d	effective diffusivity in diffusion layer for oxygen–water (cm^2 s^{-1})
D_r	effective diffusivity in reaction layer for oxygen–water (cm^2 s^{-1})
D_{hc}	hydraulic diameter of each groove (cm)
E	open circuit potential (V)
E^0	standard open circuit potential (V)
$E1$	oxygen electrode (solid carbon phase) potential (V)
$E2$	local electrolyte (liquid) potential (V)
f	friction factor
F	Faraday constant (96,500 C g^{-1} equivalent weight)
H	Henry's constant for oxygen solubility in phosphoric acid (gmol cm^{-3} atm^{-1})
i_a	local current density (A cm^{-2})
i_o	exchange current density for oxygen reduction on Pt (A cm^{-2})
i_x	current in X-direction (A)
$j(x)$	flow of cation in X-direction (A cm^{-2})
$j(y)$	flow of cation in Y-direction (A cm^{-2})
k	reaction constant of oxygen reduction reaction
l_c	groove length (cm)
m_i	product of molar flux of ith species at gas electrode interphase in X-direction and width of the cell (gmol cm^{-1} s^{-1})
m_{i0}	inlet molar flow rate of ith species (gmol s^{-1})
n	no. of electrons taking part in the reaction
n_s	grooves per manifold
$N1$	no. of agglomerate exposed per unit sqcm area in YZ-plane
p_i	partial pressure of the ith species (atm)
p_{i0}	partial pressure of the ith species at inlet (atm)
p_t	total pressure at groove inlet
R	universal gas constant (atm cm^3 gmol^{-1} k^{-1})
R_{agg}	average radius of an agglomerate (cm)
R_{orr}	oxygen reduction rate (gmol s^{-1} cm^{-3})
r	radial dimension inside an agglomerate originating at the center (cm)
T	system temperature in kelvin scale
U	oxygen reaction potential wrt the reference (V)
W	width of the cell in Z-direction (cm)
W_{max}	maximum electrical work available (W)
ΔE^0_{rev}	standard half cell potential wrt hydrogen electrode (V)

Greek letters

η	local overpotential (V)
η_0	overpotential at the bulk-electrolyte and electrode interphase (V)
κ_e	electrolyte conductivity (mho cm^{-1})
ρ_a	agglomerate density inside reaction layer (no. cm^{-3})
Ψ	flow per manifold at system temp and pressure (cm^3 s^{-1})
μ	viscosity (g cm^{-1} s^{-1})

Subscripts

1	oxygen (ith species)
2	water (ith species)

relationship between the performance of the fuel cell and various design options.

2. Phosphoric acid fuel cell (PAFC)—principle of operation

A phosphoric acid fuel cell is composed of two porous gas diffusion electrodes namely anode and cathode (see Fig. 1) [2] juxtaposed against a porous electrolyte matrix. The gas diffusion electrodes comprise a porous substrate that faces the gaseous feed. This substrate is a porous carbon paper or cloth. On the other side of this substrate, which faces the electrolyte (phosphoric acid), platinised fine carbon powder electrocatalyst is roll coated with poly-tetra-fluro-ethylene (PTFE) as a binder. PTFE also acts as a hydrophobic agent to prevent flooding of pores so that reactant gas can diffuse to the site easily. The two electrodes are separated by phosphoric acid (electrolyte; Fig. 1). At the anode, hydrogen ionizes to H^+ and migrates towards the cathode to combine with oxygen, forming water. The product water then diffuses out to the oxygen stream and comes out of the system as steam. An emf is generated between the two electrodes through conversion of reaction free energy to electricity and on connecting an external load electrical power can be extracted.

The reactions at anode and cathode are as follows [2].

At anode:

$$H_2 \rightleftharpoons 2H^+ + 2e^-, \quad \Delta E^0_{rev} = 0 \tag{1}$$

At cathode:

$$\tfrac{1}{2}O_2 + 2H^+ + 2e^- \rightleftharpoons H_2O, \quad \Delta E^0_{rev} = 1.229 \tag{2}$$

$$O_2 + 2H^+ + 2e^- \rightleftharpoons H_2O_2, \quad \Delta E^0_{rev} = 0.67 \tag{3}$$

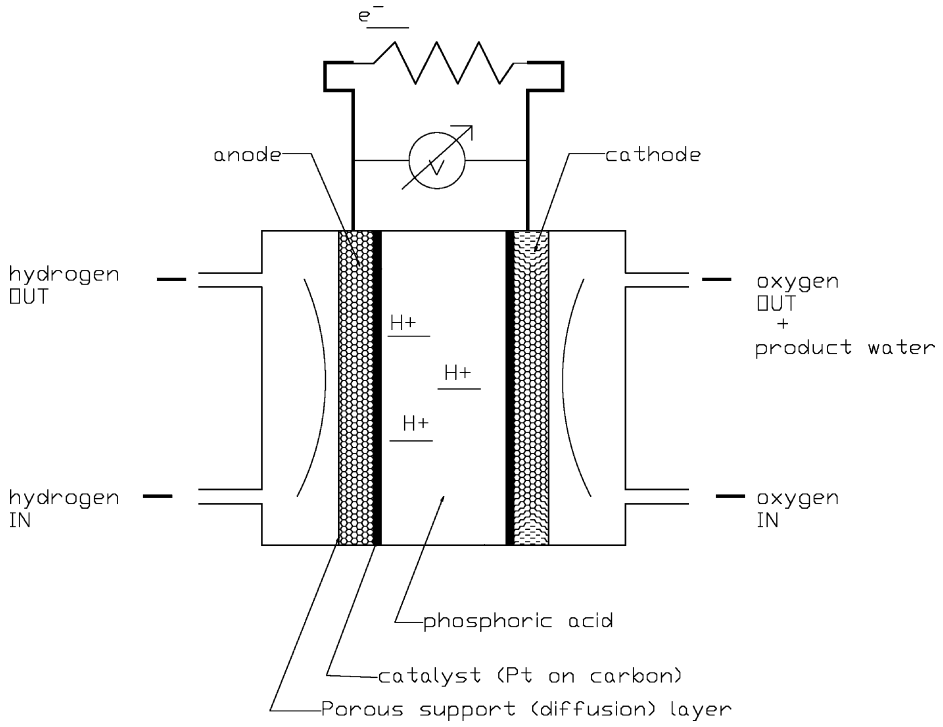

Fig. 1. Phosphoric acid fuel cell—principle of operation.

$$H_2O_2 + 2H^+ + 2e^- \rightleftharpoons 2H_2O, \quad \Delta E^0_{rev} = 1.7 \tag{4}$$

$$H_2O_2 \rightleftharpoons H_2O + \tfrac{1}{2}O_2 \tag{5}$$

Under reversible condition maximum electrical work available is [2]:

$$W_{max} = -\Delta G_{\text{water formation}} \tag{6}$$

and the ideal open circuit potential is given by Nernst equation [2]:

$$E = -\frac{\Delta G}{nF} = E^0 + \left(\frac{RT}{nF}\right) \ln\left[\frac{a_{\text{hydrogen}} a^{0.5}_{\text{oxygen}}}{a_{\text{water}}}\right] \tag{7}$$

In Fig. 2, an exploded view of a practical single cell is depicted [2] where syrupy phosphoric acid is immobilized

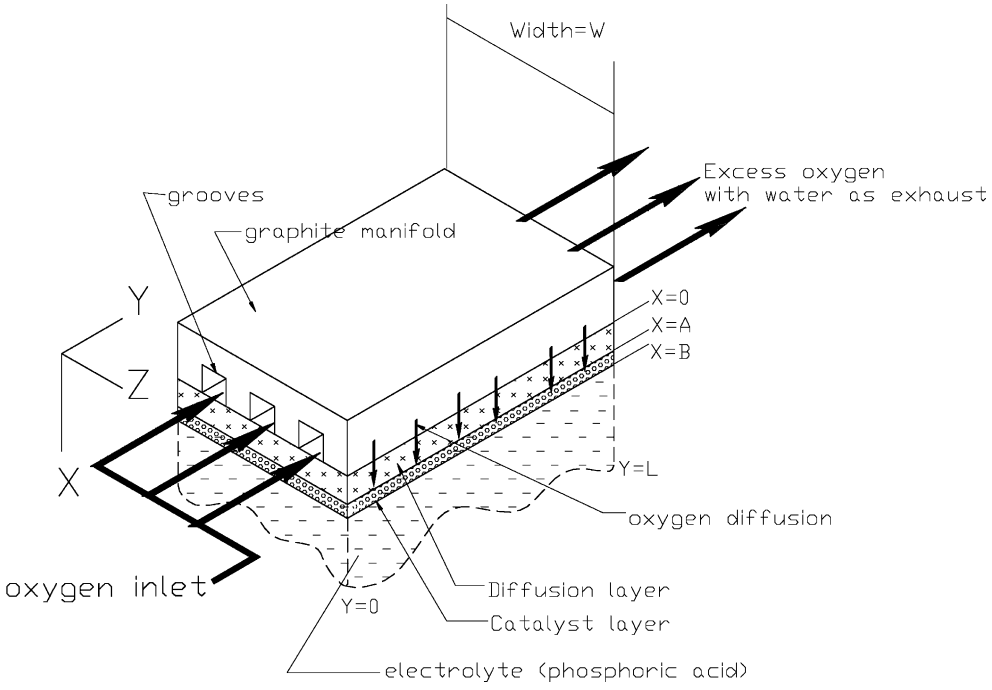

Fig. 2. Exploded view of PAFC cell.

inside a SiC matrix. The high density graphite plates as shown in Fig. 2 have grooves on one side through which reactant gases are provided to the electrodes (anode and cathode). The porous substrate of the electrodes face the grooved side of the graphite plates, whereas the catalyst is coated on the other side. In between the two electrodes, phosphoric acid is provided in silicon carbide matrix.

The whole assembly is then sandwiched between two insulator plates (not shown in the figure) and bolted tightly. The two graphite plates act as the terminals for connecting the electrical load. Such cells are stacked in series/parallel combinations for useful power. In large stacks, the graphite plates are bipolar in nature where one side of a plate provides hydrogen to one cell and the other side oxygen to the adjacent cell in series [3].

3. Background of model development

Modeling of a phosphoric acid fuel cell requires the representation of the following factors in the model: (i) temperature, (ii) operating pressure, (iii) humidity, (iv) electrical load, and (v) phosphoric acid management inside PAFC.

PAFC electrodes are basically porous gas diffusion electrodes (GDE), which are difficult to characterize on a microscopic level. One approach to this problem is to employ a macroscopic model like ‘‘porous electrode theory’’ [1,4] that accounts for the essential features of a porous electrode without going into the exact geometric details. GDEs like that of a PAFC adds an additional degree of complexity due to presence of three phases, viz. gas, electrolyte and catalyst surface. This requires a model with dual porosity, one each for the gas phase and the electrolyte phase. One approach is to employ ‘‘flooded agglomerate’’ concept, first introduced by Giner and Hunter [5]. A modified version of this concept was exploited for the development of the model in this work as described later. The main advantage of considering this concept is its easy adaptability to electrode made by various methods. It should be recognized that the flooded agglomerate model, when executed correctly, is essentially a discretized version of ‘‘porous electrode theory’’ [1].

Fig. 2 shows the cross-section of a composite cathode. Bulk gas, i.e. oxygen, flows in the Y-direction through the ribbed support over the left side of the electrode. As the gas flows, part of the oxygen diffuses through the porous substrate of the electrode. The diffusion of oxygen is in X-direction. The gas after passing through porous substrate (diffusion layer) reaches the catalyst layer also termed as reaction layer. Catalyst layer is a porous layer partly filled with electrolyte. The gas diffuses through the dry pores, dissolves in the electrolyte and then diffuses to the catalytic site. Oxygen reduction takes place on the site and the product water back diffuses through the diffusion layer to escape in the oxygen stream.

Most of the published literature deals with one-dimensional models for PAFC cathode. This is valid, provided the throughput of the gas is quite high inside the cell, so that the change in concentration of the gas in Y-direction is negligible. However for a big cell with limited throughput of gas, concentration of oxygen changes substantially in Y-direction owing to depletion of oxygen and back diffusion of product water. This leads to the necessity for developing a two-dimensional model for the oxygen electrode, considering no changes in Z-direction. This condition is valid for most of the cell as the gas feeding is done by parallel grooves along Z-direction.

It is generally accepted that the major difficulty in fuel cell development lies with the kinetics of the oxygen electrode [2,6]. The hydrogen electrode kinetics is relatively much faster than that of the oxygen electrode. Most of the researchers modeling fuel cells have considered primarily two aspects, viz. diffusion of gases to electrode surface and kinetics of the oxygen electrode. To the best knowledge of the authors, two-dimensional models for PAFC cathode in the literature have been minimal. But many two-dimensional models have been proposed for other types of fuel cells. Typically, two-dimensional models are developed to study and analyse various issues concerning the fuel cell, e.g. electrocatalyst utilization, current density distribution, hydrodynamics, etc. Boersma and Sammes [7] have analysed the distribution of gas flow in internally manifolded solid oxide fuel cells (SOFC). Kulikovsky et al. [8] have considered a two-dimensional model to study the dead and active reaction zones in the cathode compartment of a polymer electrolyte membrane (PEM) fuel cell. Dutta et al. [9] have used a three-dimensional flow model to analyse the effects of membrane thickness and cell voltage on the axial distribution of current density and rate of water transport in PEM fuel cells.

A number of two-dimensional models for proton exchange membrane fuel cell (PEMFC) have also been published, the applications of which have been varied—to study water transport [10]; influence of ohmic drop within the active layer on electrode performance [11]; calculation of cell performance, ohmic resistance and water profile in the membrane, current distribution and variation of temperature along the gas channels [12]; hydrodynamics of the gases and multicomponent transport in the cathode [13]; a computational fluid dynamics (CFD) based model to account simultaneously for electrochemical kinetics, current distribution, hydrodynamics, multicomponent transport and hydrogen dilution effects [14]; two-dimensional, two-phase, multicomponent transient model [15].

Some of the above-mentioned issues are also studied for direct methanol fuel cells (DMFC) [16–18] and molten carbonate fuel cells (MCFC) [19–21]. To undertake a comprehensive study and a detailed analysis of PAFCs, as a first step in the process engineering, we present a two-dimensional steady-state model in this work. The model has been used to study the effects of various process parameters on the

performance of PAFC and gain insight into the different phenomena occuring in PAFCs to help in carrying out further advanced studies like control and diagnostics.

4. Development of steady state model for PAFC cathode (oxygen electrode)

Diffusion of Oxygen and back diffusion of water vapor in the porous substrate, where no reaction takes place, can be defined by the following governing equation:

$$\left(\frac{D_d}{RT}\right)\left(\frac{\partial^2 p_i}{\partial x^2}\right) + \left(\frac{D_d}{RT}\right)\left(\frac{\partial^2 p_i}{\partial y^2}\right) = 0, \quad i = 1, 2 \tag{8}$$

Modeling of the reaction layer can be done by using the flooded agglomerate model [1,4] coupled with gas diffusion equations.

Fig. 3 depicts the concept of flooded electrolyte model [1]. It is considered that the carbon particles containing catalyst (Pt) formed small agglomerates. These agglomerate globules are completely flooded with electrolyte (phosphoric acid). The inter agglomerate space is partially filled with electrolyte due to the presence of PTFE. Reactants (oxygen) can diffuse through this inter agglomerate space and can reach the agglomerate surface. The reactant is consumed in the agglomerates and product water diffuses out from the agglomerate surface. Diffusion of gas in electrolyte medium is inside the agglomerates only. Although the size of the agglomerate particle may be somewhat uncertain and may vary with position, still this model gives a good account of the processes involved and can be adopted easily to different types of electrodes.

The following assumptions are made in the model development [1,4]:

- Spherical agglomerates.
- Agglomerate size $\ll$ thickness of the active reaction layer.
- No ohmic loss inside carbon particles.

Hence, oxygen transport inside the spherical agglomerate undergoing reaction can be written as [1]:

$$\left(\frac{D_{agg}}{r^2}\right)\frac{\partial}{\partial r}\left(\frac{r^2 \partial c_{1a}}{\partial r}\right) = -R_{orr} \tag{9}$$

with the following boundary conditions [1]:

$$r = R_{agg}, \quad c_{1a} = c_{os} \tag{10}$$

$$r = 0, \quad \left(\frac{\partial c_{1a}}{\partial r}\right) = 0 \tag{11}$$

Since all fuel cell operations are carried out much away from equilibrium, that is the overpotential is always

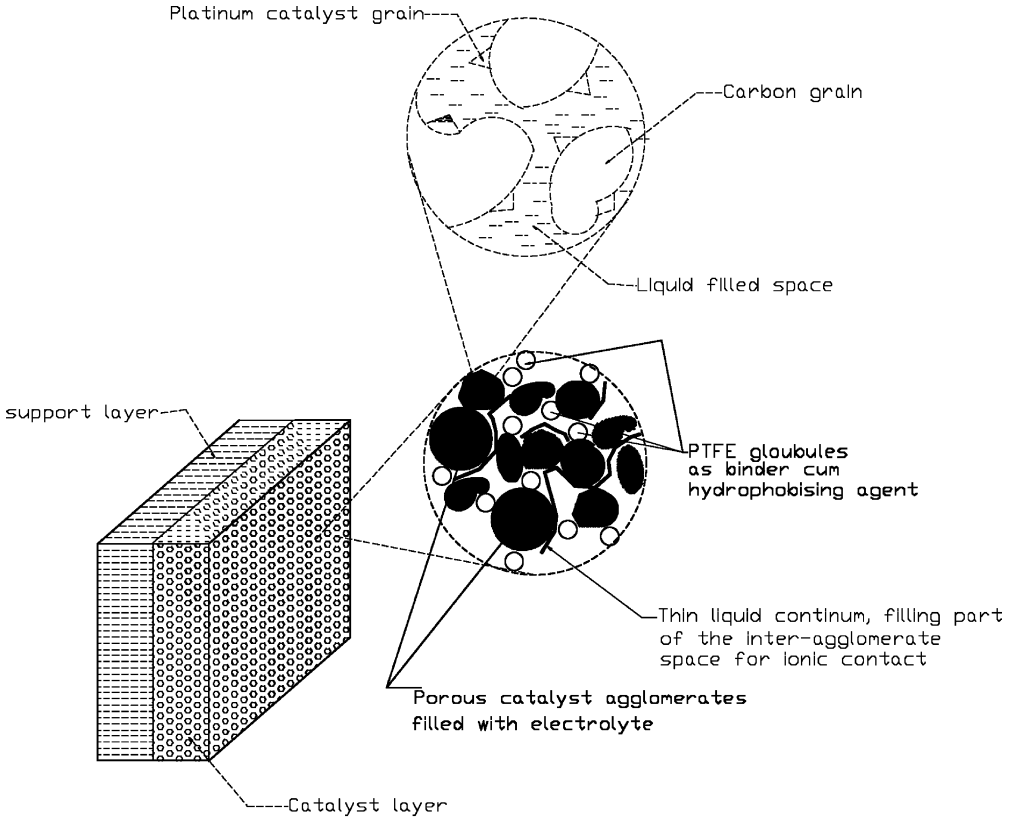

Fig. 3. Flooded electrolyte model.

>75 mV, R_{orr} in equation (9) can be assumed to exhibit Tafel kinetics:

$$-R_{orr} = \frac{a_a i_a}{nF} = \left(\frac{a_a i_o}{nF}\right)\left(\frac{c_{1a}}{c_{os}}\right)\exp\left(-\frac{2.3\eta}{b}\right) = (a_a k c_{1a})\exp\left(-\frac{2.3\eta}{b}\right) \quad (12)$$

where $k = i_o/(nFc_{os})$.

Eq. (9) and (12) along with the boundary conditions, Eqs. (10) and (11), can be analytically solved to give [1,22]:

$$c_{1a} = c_{os}(R_{agg/r})\frac{\sinh(\phi(r))}{\sinh(\phi(R_{agg}))} \quad (13)$$

where

$$\phi(r) = \sqrt{\frac{a_a k}{D_{agg}}}r\exp\left(-\frac{2.3\eta}{2b}\right) \quad (14)$$

The molar flux of oxygen (N_{oxy}) at the surface of an agglomerate can be estimated from Eq. (13) as

$$N_{oxy} = -\left(\frac{1}{R_{agg}}\right)D_{agg}c_{os}[\phi(R_{agg})\coth(\phi(R_{agg})) - 1] \quad (15)$$

Henceforth, consumption of oxygen per unit volume at any point inside the reaction layer can be determined by the product of agglomerate density, single agglomerate surface area and N_{oxy}. Therefore the governing equation for oxygen balance in the reaction layer can be written as

$$\left(\frac{D_r}{RT}\right)\left(\frac{\partial^2 p_1}{\partial x^2}\right) + \left(\frac{D_r}{RT}\right)\left(\frac{\partial^2 p_1}{\partial y^2}\right) = \Gamma \quad (16)$$

where

$$\Gamma = 4\pi\rho_a D_{agg}R_{agg}c_{os}[\phi(R_{agg})\coth(\phi(R_{agg})) - 1] \quad (17)$$

$$\phi(R_{agg}) = \sqrt{\left(\frac{a_a k}{D_{agg}}\right)}\left[R_{agg}\exp\left(-\frac{2.3\eta}{2b}\right)\right] \quad (18)$$

and

$$c_{os} = Hp_1 \quad (19)$$

Distribution of overpotential inside the catalyst layer can be estimated by considering ohmic law for the cation flow, in this case hydrogen ions, in the electrolyte filled zone [4]. Thus, change of overpotential in X-and Y-direction can be related to the current flux as follows:

$$\frac{\partial\eta}{\partial x} = -\frac{j(x)}{\kappa_e A^* N1} \quad (20)$$

$$\frac{\partial\eta}{\partial y} = -\frac{j(y)}{\kappa_e A^* N1} \quad (21)$$

Considering a small control volume of Δx and Δy ($\lim \Delta x, \Delta y \to 0$) inside the catalyst layer and balancing the charge flow across it yields

$$\frac{\partial j(x)}{\partial x} + \frac{\partial j(y)}{\partial y} = -nF\Gamma \quad (22)$$

Differentiating Eqs. (20) and (21) and substituting them in Eq. (22) gives

$$\frac{\partial^2\eta}{\partial x^2} + \frac{\partial^2\eta}{\partial y^2} = \frac{nF\Gamma}{\kappa_e A^* N1} \quad (23)$$

Cation flow, i.e. hydrogen ion flow in the catalyst layer depends upon the local electrolyte conductivity which in turn depends upon the local phosphoric acid concentration. A non-linear curve was fitted to co-relate electrical conductivity and phosphoric acid concentration from the data available in the literature [23] as shown in Eq. (24).

$$\kappa_e = 0.72796 - 6.5068\exp(-07)c_{H_3PO_4} \quad (24)$$

It is assumed that the concentration of acid inside the agglomerates remain constant and the local partial pressure of the acid immediately outside the agglomerate is in equilibrium with the acid inside the agglomerate. Considering this, the phosphoric acid concentration and equilibrium vapor pressure at system temperature was co-related from the data available in the literature [24]. The best fitted curve is shown in Eq. (25).

$$c_{H_3PO_4} = \frac{1}{0.008623 + 0.004187p_2^{0.5}} \quad (25)$$

Water transfer inside the catalyst layer can be depicted by considering the fact that local water generation due to reaction diffuses out towards the bulk gas alongwith evaporated moisture from the bulk acid catalyst layer interphase. Thus, local acid concentration changes depending upon the position from the bulk gas electrode interphase and the local current density. Higher current density means more dilution of acid, however, proximity to bulk gas zone or diffusion layer implies drier environment. Considering negligible mass transfer resistance from bulk to agglomerate surface due to intimate positioning, partial pressure of water vapor at agglomerate surface remains same as that of the bulk phase in the catalyst layer. Therefore, the water transport phenomena in the catalyst layer can be modeled by the following equation:

$$\left(\frac{D_r}{RT}\right)\left(\frac{\partial^2 p_2}{\partial x^2}\right) + \left(\frac{D_r}{RT}\right)\left(\frac{\partial^2 p_2}{\partial y^2}\right) = 2\Gamma \quad (26)$$

4.1. Boundary conditions

Oxygen diffusion rate through the porous layer is determined by the rate of consumption of the gas in the catalyst layer as well as the concentration of the gas at bulk. Depending upon the flow rate, bulk oxygen concentration changes along the Y-direction (Fig. 2). Also back diffusion of water vapor changes the concentration profile inside the

porous substrate. Taking into consideration all these effects, the system can be solved as a boundary value problem. However, concentration profile along the bulk flow direction is not known, as it is determined by the inlet flow rate, composition, pressure drop along the bulk flow channel and the diffusion rates of the reactant and product. To overcome this problem an initial guess value of the concentration profile in the bulk could be given. After one set of computation is over, this profile may be corrected from the diffusive fluxes at different positions in the bulk flow direction. This process may be continued till the profile does not change further.

Considering a uniform pressure profile as initial guess for oxygen and water vapor:

$$p_1 = p_{10}, \quad \text{at } x = 0, \forall y$$

$$p_2 = p_{20}, \quad \text{at } x = 0, \forall y$$

After one set of computation, $\partial p_i/\partial x$ at $x = 0, \forall y$ is determined. Considering a control length of Δy on the bulk-porous layer interface and taking mass balance over it and defining m_i as the product of molar flux of ith component at the bulk gas-electrode interface and width of the electrode, W (refer Fig. 2):

$$m_i = W\left(\frac{D_d}{RT}\right)\left(\frac{\partial p_i}{\partial x}\right)_{x=0,y}, \quad i = 1, 2 \tag{27}$$

Considering pressure drop along the flow channel due to hydraulic resistance (Fig. 2), partial pressure along Y-at $X = 0$ can be rewritten as

$$p_{i;x=0,y} = p_t \frac{\int_0^y m_i \, dy + m_{i0}}{\sum_{j=1}^{2} \int_0^y m_j \, dy + m_{j0}}, \quad i = 1, 2 \tag{28}$$

In order to find out the local total pressure along the bulk gas electrode interphase it may be considered that the flow inside the channel is in laminar zone. This is generally valid for the planar structure fuel cells upto a flow length of 1 m [25]. It can be also checked by determining the actual Reynolds number for specific cases. Thus, considering Poiseuille flow:

$$\Delta p = K_c \Psi \tag{29}$$

where $K_c = f\mu l_c/n_s a_c D_{hc}^2$.

Ψ being local flowrate per cell at system temperature and pressure; f is the friction factor which depends on the channel geometry, i.e. $f = 28.4$ for square cross-section [25]. Thus, after every set of computation, the partial pressure of water vapor and oxygen can be updated along the bulk flow direction till the profile remains unchanged. To provide the boundary conditions for water transport equation inside the electrode, it can be considered that at electrode and bulk acid interphase the gas remains saturated with bulk acid concentration.

At $x = B, \forall y$:

$$p_2 = p_{2sat} \quad \text{(BC 1)}$$

As shown in Fig. 2, at inlet entire electrode cross-section is exposed to the incoming stream.

At $y = 0, \forall x$:

$$p_1 = p_{10} \quad \text{(BC 2)}$$

$$p_2 = p_{20} \quad \text{(BC 3)}$$

At $y = L, \forall x$

$$\frac{\partial p_1}{\partial y} = 0 \quad \text{(BC 4)}$$

$$\frac{\partial p_2}{\partial y} = 0 \quad \text{(BC 5)}$$

Boundary conditions 4 and 5 (BCs 4 and 5) are justified by the fact that at the end of the electrode entire cross-section is blocked with the sealant and no material transfer takes place across the cross-section.

At $x = B, \forall y$:

$$\frac{\partial p_1}{\partial x} = 0 \quad \text{(BC 6)}$$

BC 6 is valid considering no oxygen transport beyond the electrode's catalyst layer. The reference potential is the hydrogen electrode which is placed after the catalyst layer of the oxygen electrode separated by the acid electrolyte. Hence, the overpotential measured in reference to it can be considered as the overpotential at the end of the oxygen electrode catalyst layer (BC 7).

At $x = B, \forall y$:

$$\eta = \eta_0 \quad \text{(BC 7)}$$

At $x = A, \forall y$:

$$\frac{\partial \eta}{\partial x} = 0 \quad \text{(BC 8)}$$

At $y = 0, A < x < B$:

$$\eta = \eta_0 \quad \text{(BC 9)}$$

BC 8 is considered since ion movement takes place only inside the electrolyte filled catalyst layer and not in the dry diffusion layer.

At $y = L, A < x < B$:

$$\frac{\partial \eta}{\partial y} = 0 \quad \text{(BC 10)}$$

4.2. Model solving and validation

The model developed was numerically solved using Pdease2D. Pdease2D is a finite element software for solving two-dimensional linear/non-linear partial differential equations. Pdease2D solves simultaneous PDE using Galarkin finite element method. It has adaptive grid control mechanism built in. Since the electrode structure is composed of two layers it was so programmed that the variables are continuous at the layer interfaces. Macsyma programming

language platform was used for customizing and interfacing with peripheral software.

The set of equations are solved with a given overpotential at the electrolyte side. Further, integrating the molar flux of oxygen in X-direction along the bulk gas–electrode interface and multiplying by width of the cell, W, total oxygen inflow can be found. Once the molar flux of oxygen has been determined, total current generated can be calculated as

$$\text{gross current} = nFW \int_0^{l_c} m_1 \, dy \tag{30}$$

Thus, the steady state overall current generated against a given overpotential and oxygen flow rate with inlet humidity can be determined.

The model developed was first tried in one-dimensional mode to see the validity of the basic parameters. In order to test this a micro setup known as ''unit cell'' was used where the flowrate kept is such that there is no concentration gradient along the bulk flow interphase. After this further tests were carried out in experimental stacks, details of which are provided in the following section and difference between one-dimensional and two-dimensional model was analysed.

4.2.1. Experimental setup for model validation

To validate the model in one-dimension, i.e. ''X-direction'', the ''unit cell'' setup is used. It consists of a single cell of one cathode and one anode separated by acid layer. The area of the exposed electrode is very small so that the concentration of the gas at any point over the electrode surface remains same. The electrodes were connected through a ''PARC'' potentiostat galvanostat with EG & G developed electrochemical experimentation software. The sketch of the experimental setup is shown in Fig. 4. A hydrogen electrode is used as the reference point for the measurement. This arrangement allows independent readings of each electrodes. The detail design, being proprietary of NMRL, is not discussed here.

To validate the model in two-dimensional form, an average of four identical experimental phosphoric acid fuel cell stack each consisting of four cells were used. In effect an overall average of 16 cells separated in four groups were used for model validation. All the components of the stack were developed in house at NMRL.

A conceptual sketch of the stack and the components are shown in Fig. 5. As shown in the figure, two types of groove design were used, types A and B. The electrodes were made by roll coating catalyst powder on hydrophobised porous TGP-120 graphite paper. The catalyst used was Pt loaded on Vulcan-XC72R carbon. Teflon suspension of particle size range ∗–∗ was used as a binder and hydrophobic agent to prevent flooding of pores in the catalyst layer. In between the two electrodes, a silicon carbide matrix was incorporated to hold syrupy concentrated phosphoric acid.

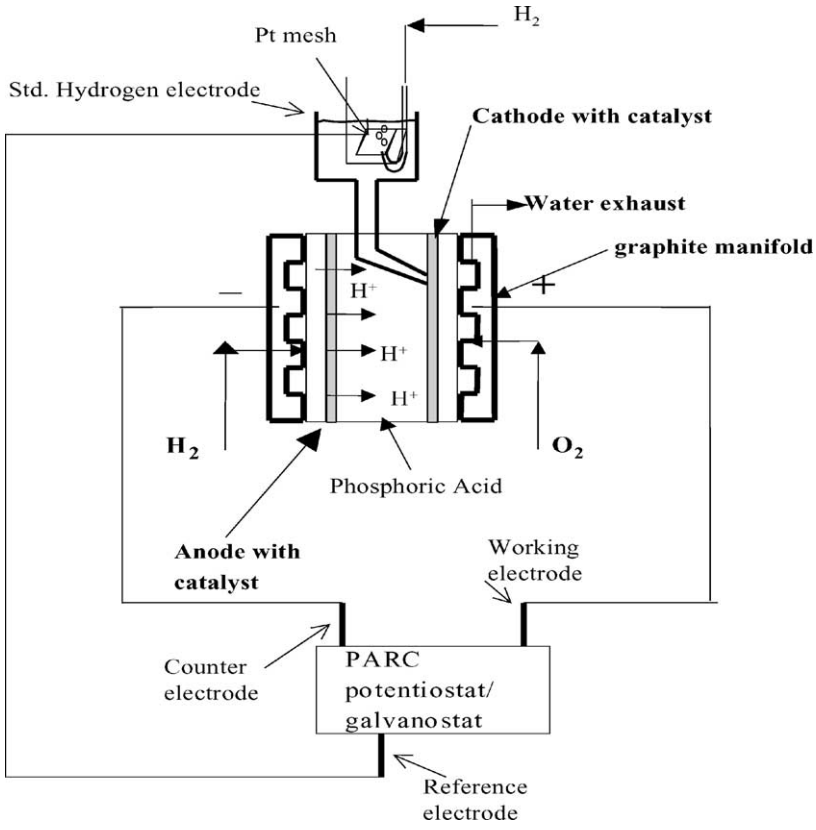

Fig. 4. Unit cell experimentation setup.

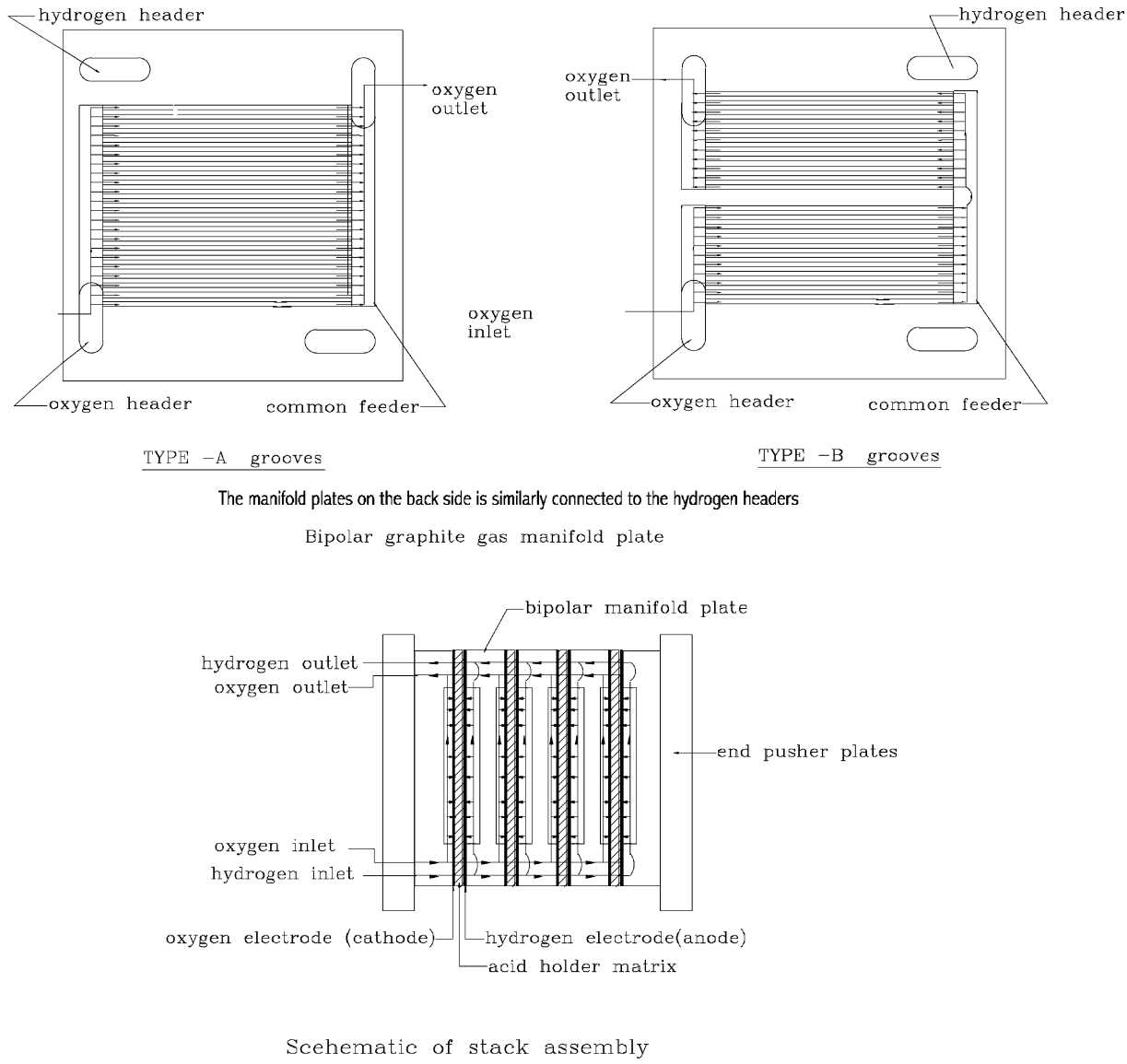

Fig. 5. Experimental stack components and assembly scheme.

In a stack, all the cells are electrically connected in series and the reactant gases, viz. humidified hydrogen and oxygen are provided through common headers to each cell. Similarly, all the outlets are connected to another common header through which the lean gas flows out. In order to eliminate maldistribution of gases in the cells in a stack, fewer number of cells (four cells) were assembled with extra large feeder holes. The assemblage was done like a plate and frame filter press assembly. Conceptual flow pattern of gases inside the stacks is shown in Fig. 5. Each cell is characterised as

- effective electrode area = 100 cm^2;
- groove type A = straight grooves, all parallel, gas travel length = 10 cm, width = 10 cm;
- groove type B = groove tortuous and are carried over from inlet to outlet, gas travel = 20 cm, width = 5 cm.

Schematic of the complete experimental setup is shown in Fig. 6. Pure hydrogen and oxygen gases were used from the cylinders. The hydrogen was humidified with predetermined humidity level, in order to prevent drying up of acid, while the oxygen was used directly. In the outlet streams, humidity levels of hydrogen and oxygen was checked using dry and wet bulb methods. Emf of all the cells were measured using precision voltmeter and the circuit current was measured using shunt based ammeter. Experimentation was done by keeping the overall stack voltage at a predetermined value. In order to operate the system at such potentiostatic mode a dc compensator was used in series with the stack. An average of all the four cells in series is taken as the cell potential.

Parameters like agglomerate radius, agglomerate density are determined through scanning electron micrographs of

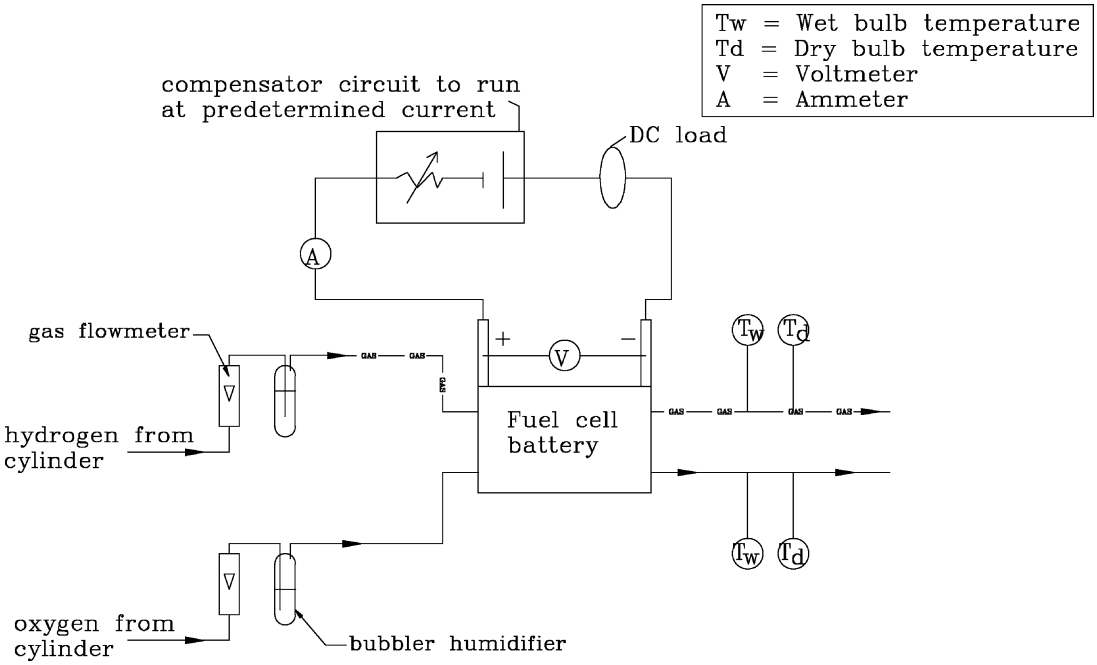

Fig. 6. Experimental setup for steady state model validation.

the electrodes. Other parameters like "Tafel slope", and active area per unit volume of agglomerate etc, are tuned to match the model output to some standard experimental results from small test PAFC stacks. Table 1 lists the final values of the parameters used for simulating the actual stacks.

4.2.2. Analysis of data for model validation

Experimental runs were taken on the unit cell to check the model's one-dimensional prediction. To simulate one-dimensional effect the concentration along the bulk gas flow is kept unchanged. Fig. 7 depicts experimental and simulated values at various overpotentials. The values match quite well and as expected the current increases rapidly with overpotential as the reaction rate increases exponentially with respect to the overpotential, refer Eq. (12).

Several experimental runs were taken under various flow rates and output potential settings. On the hydrogen side, flow rate was always kept twice the oxygen flow rate to maintain adequate pressure differential. Temperature of the fuel cell was maintained at 150 °C. The oxygen inlet was maintained at 0% humidity and the hydrogen inlet was saturated with moisture at 60 °C. The reason for maintaining this particular saturation level at hydrogen inlet is that the target acid concentration inside the cell is around 90–95% H_3PO_4. The partial pressure of water over this acid at 150 °C matches that of the water vapor pressure at 60 °C. In order to minimize loss of moisture at hydrogen side, the gas is moistened accordingly.

Fig. 8 depicts experimental and simulated current for type A grooves at different oxygen flowrates. As expected with increase in flowrate the current increases. The dotted line shows the current predicted by the model under infinite oxygen flow, i.e. if a single dimension model without the partial pressure drop along the groove is considered.

Fig. 9 shows a similar current vs oxygen flowrate plot of experimental and simulated values for type A grooves at a lesser overpotential of 0.3 V per cell. Here, it can be

Table 1
Values of parameters

Parameter name	Value	Remark
A^*	πR_{agg}^2 (cm^2) of projection in YZ-plane	Literature
a_a	3.5E−04 (cm^2 cm^{-3}) of agglomerate	Experimental
b	120 mV per decade	Tuning
D_{agg}	1.0E−04 (cm^2 s^{-1})	Literature
D_r	0.2E−03 (cm^2 s^{-1})	Literature
Diffusion layer	400 μm thick	Experimental
E	0.92 V	Experimental
H	5.5E−08 (gmol cm^{-3} atm)	Literature
i_o	1.0E−06 (A cm^2)	Literature
n	4	Stoichiometry
R_{agg}	1.0E−04 (cm)	SEM picture
Reaction layer	400 μm thick	Experimental
T	150 + 273 K	Experimental
W	10 cm	Experimental
κ_e	Function of phosphoric acid concentration	Model
ρ_a	$0.5/\pi R_{agg}^2$	Literature
λ_d	0.5	Experimental
λ_r	0.5	Experimental
a_c	0.2 cm^2	Experimental
n_s	13 grooves per manifold (type A)	Experimental

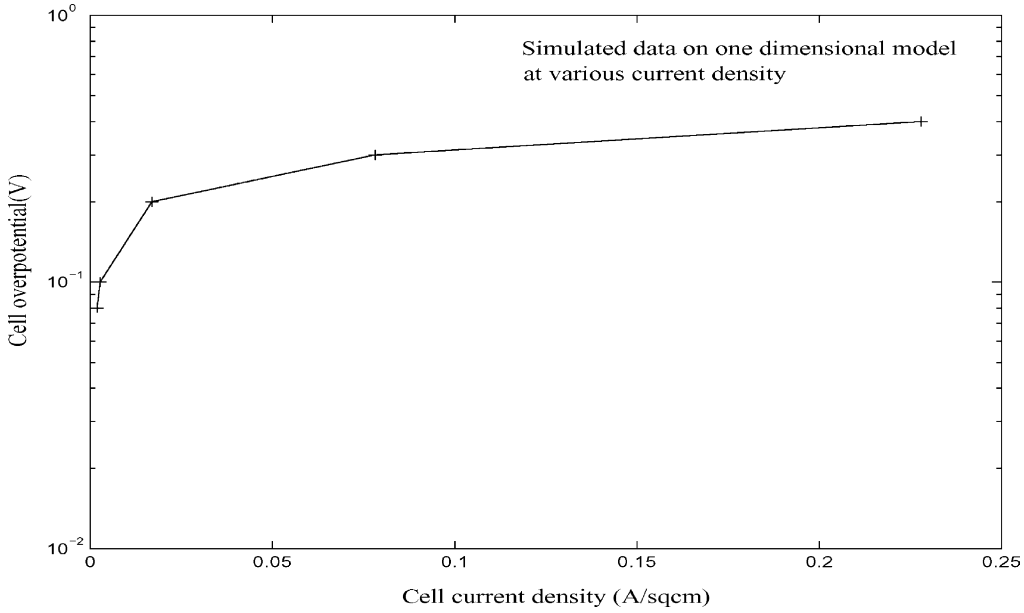

Fig. 7. One-dimensional model validation with unit cell data.

seen that the trend is similar and the one-dimensional approach would have predicted a higher value than the actual.

Figs. 10 and 11 show the moisture taken up by the oxygen. It can be seen that the water evaporated is much higher than the water generated at the cathode due to reaction. The dotted line depicts the theoretical water generation due to reaction, determined from the total experimental current. It can be also seen that the water evaporation from the acid layer is almost independent of the current or overpotential and depends primarily upon the gas flow rate. This is possibly due to much higher water uptake of oxygen than water generated which makes the outlet gas almost saturated.

The other type of groove pattern on which the validation runs were taken was "type B" grooves as shown in Fig. 5. The trend for this groove pattern remains same as expected with increase in current with flowrates. Requirement to explore various kinds of groove patterns and their efficacy comparison with the help of the steady state model are discussed in the Section 4.4. Fig. 12 shows current vs flowrate data at an overpotential of 0.3 V for type B grooves.

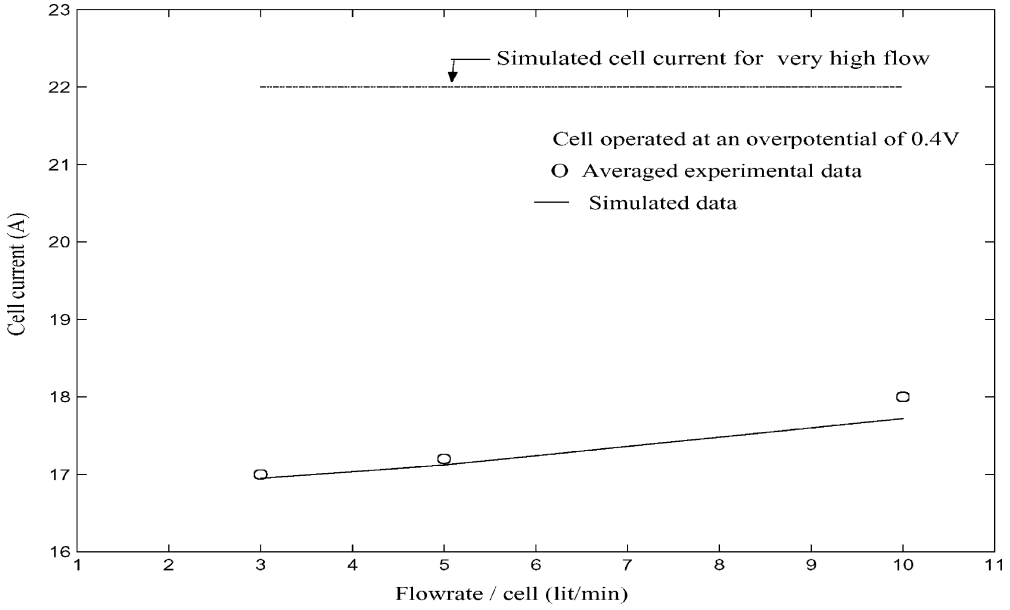

Fig. 8. Validation data for steady state model—type A groove.

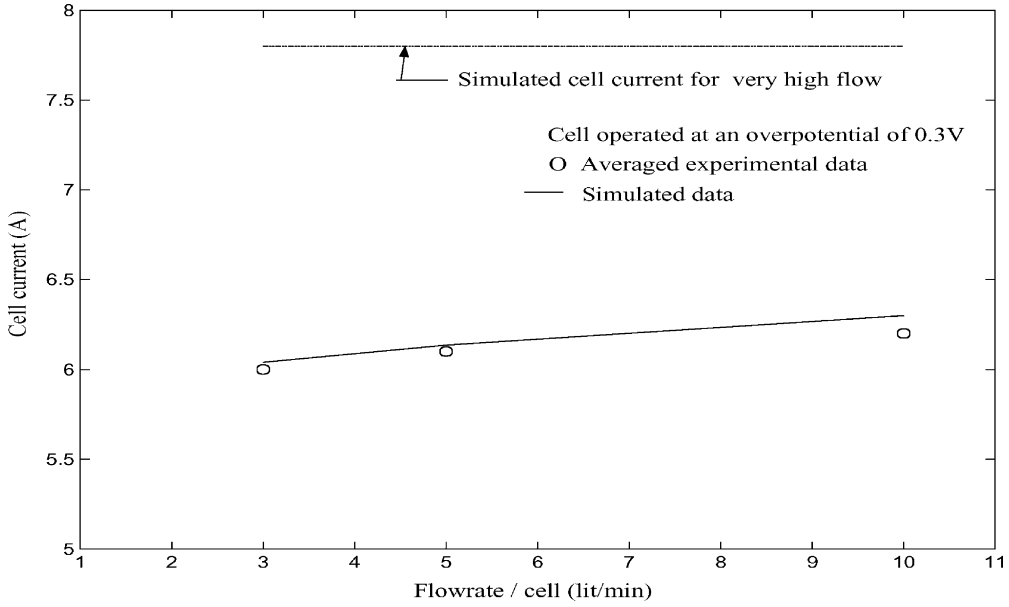

Fig. 9. Validation data for steady state model—type A groove.

The current value at various flowrates of oxygen shows marginal improvement.

4.3. Parameter sensitivity analysis

The complete list of parameters and the actual values used for the model validation is referred in Table 1. Values of some of these parameters like diffusion coefficients, vapor pressure, porosity etc were taken from the literature. Parameters like electrode thickness, catalyst surface area, agglomerate diameter, etc. were determined experimentally. It is essential to determine the dependency of the model output on the accuracy of the parameters. Many of the parameters used in this model cannot be determined very accurately, like exchange current density, active area of catalyst, etc. A range which often extends in decades are possible for many of these parameters. Secondly, for tuning of the model, to represent the experimental data, parameter sensitivity is essential. Apart from that, estimating output behavior of a validated model provide useful insight for the actual system improvement.

Of the parameters used in the model, Tafel slope shows highest sensitivity towards model output. In order to test this parameter very high flowrates of oxygen were considered

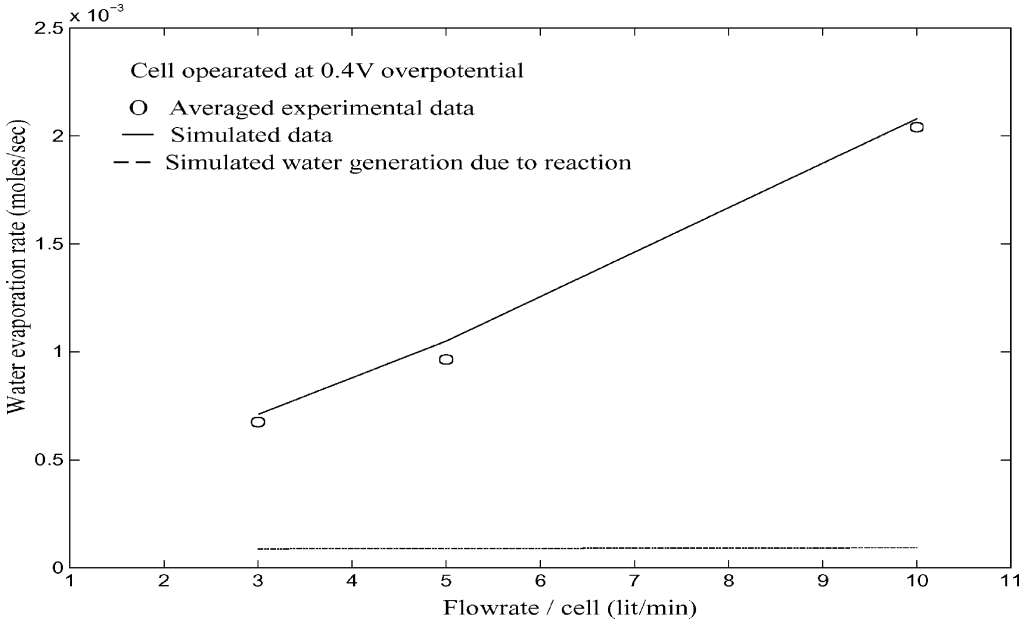

Fig. 10. Moisture loss in oxygen side at 0.4 V ovepotential—type A groove.

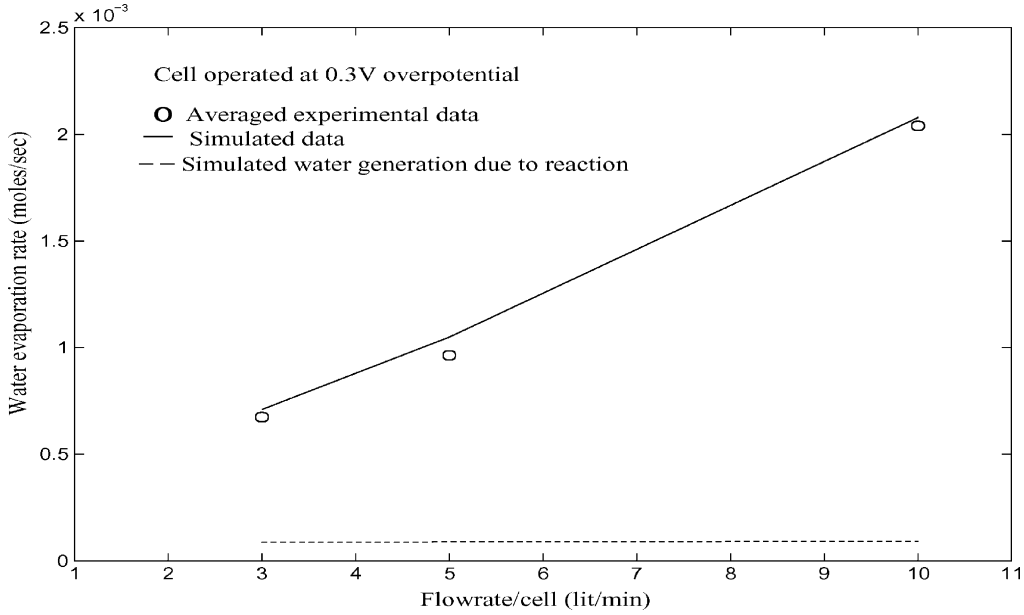

Fig. 11. Moisture loss in oxygen side at 0.3 V overpotential—type A groove.

which eventually makes the system free from the effects of operating conditions like gas flow rate and inlet humidity. It was found that a change of Tafel slope value from 0.11 to 0.12 V per decade causes the output current density to change from 300 to 220 mA per sqcm as shown in Fig. 13. The other parameter which shows strong dependency is active catalyst area per unit volume of agglomerate (a_a), as shown in Fig. 14. The effect of the same on current output is almost linear as expected.

The diffusion resistance inside agglomerate decreases with agglomerate size resulting in increase of current as shown in Fig. 15. Dependency of current on agglomerate size is found to be less sensitive. Oxygen exchange current density, i.e. the rate of reaction per unit area of catalyst surface represented in the form of current at equilibrium is a debated one as it strongly depends upon the nature of Pt crystal structure, presence of various forms of platinum oxide, etc. [2,26]. Various exchange current density were tried and the results are shown in Fig. 16.

4.4. Utility of the model

The two-dimensional steady state model found its utility primarily in fuel cell component design. With this two-

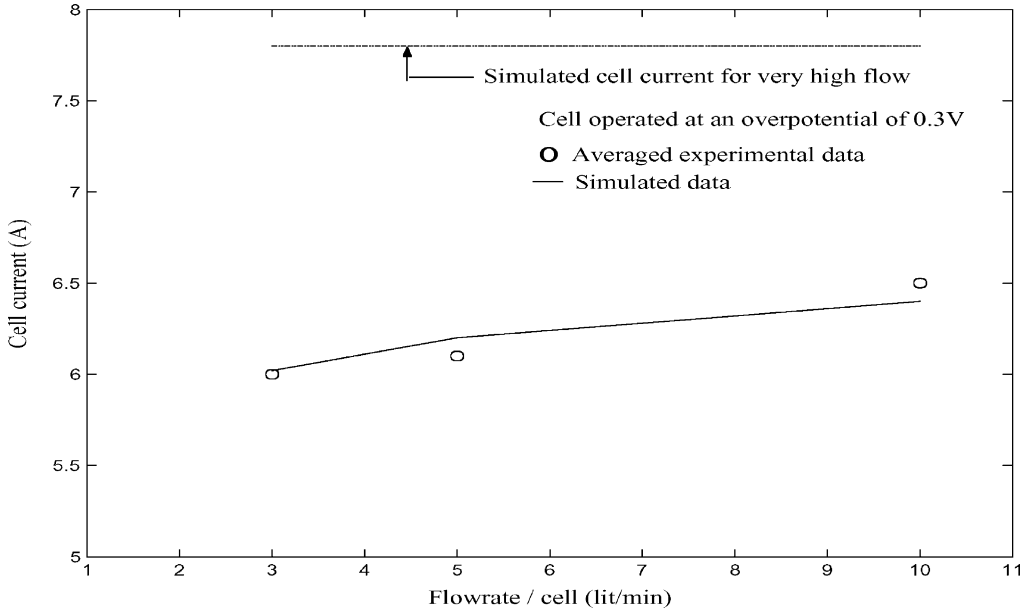

Fig. 12. Validation data for steady state model- type B groove.

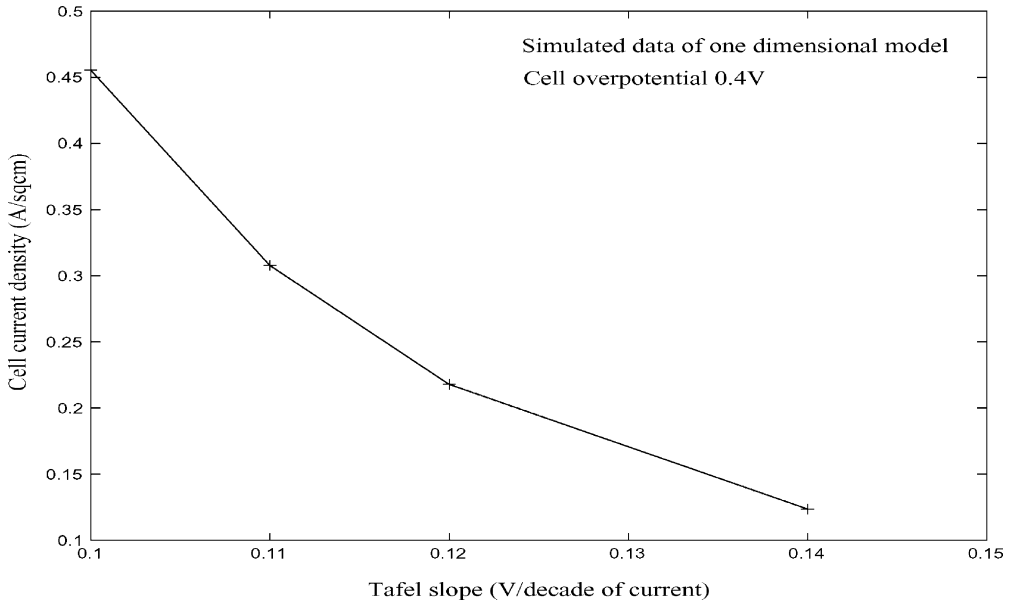

Fig. 13. Effect of Tafel slope on electrode performance.

dimensional model one can analyse the various sections of an electrode and can study the variation of reaction rates at different places. This helps in improvement and scale up of components like electrode shape factors, reduction of diffusional resistance, optimum catalyst layer thickness, etc.

4.4.1. Groove design

The groove pattern on graphite manifold plates helps in proper distribution of gases and can be designed for better cell performance. For example, the simple type A groove causes drop in stack current at low flowrates. This requires enhanced flowrates which cause loss of excess oxygen. To reduce the losses one can split the gas flow into a narrower flow width and increase the flow path length. Type B groove pattern is a step towards this direction, however, a large increase in path length may cause higher hydraulic pressure drop. The Figs. 9 and 12 show marginal improvement of current over type A grooves.

On analysis of the partial pressure contour from the model, the major concentration gradient starts at the interphase of catalyst and diffusion layer. To overcome this a proprietary ‘‘jump over’’ groove design is developed at

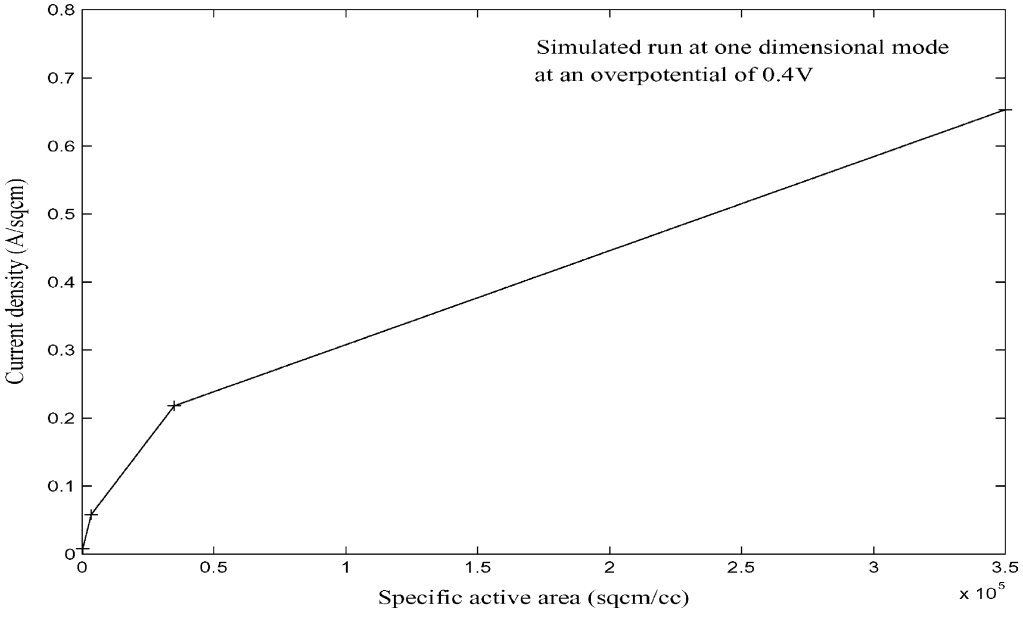

Fig. 14. Effect of active catalyst area on electrode performance.

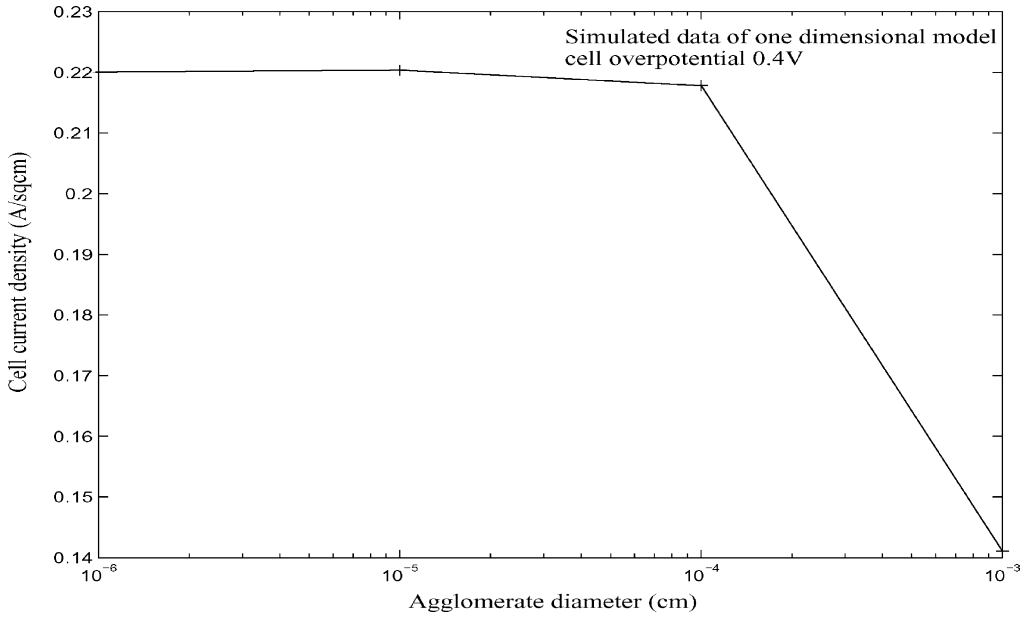

Fig. 15. Effect of agglomerate size on electrode performance.

NMRL and analysed with this model. The final pattern yields around 20% higher current than that of type A grooves at low flowrate.

4.4.2. Catalyst layer thickness

As the catalyst layer thickness increases the catalyst loading and, hence, the total number of reaction sites increase. However, with increasing thickness the resistance of cation to flow inside the catalyst layer increases. The effect of catalyst thickness on current density at a fixed overpotential has been studied using the model which shows that a catalyst layer of around 400–500 μm is sufficient for the electrode performance.

4.4.3. Humidity control

Control of cell humidity under steady state operation is generally done by humidifying the hydrogen gas, slightly higher than the equilibrium water vapor pressure of the target acid concentration at the fuel cell temperature. The oxygen is generally fed dry. This creates a problem, as the amount of water loss from acid in the oxygen stream is quite high (refer Fig. 10). This causes problems associated

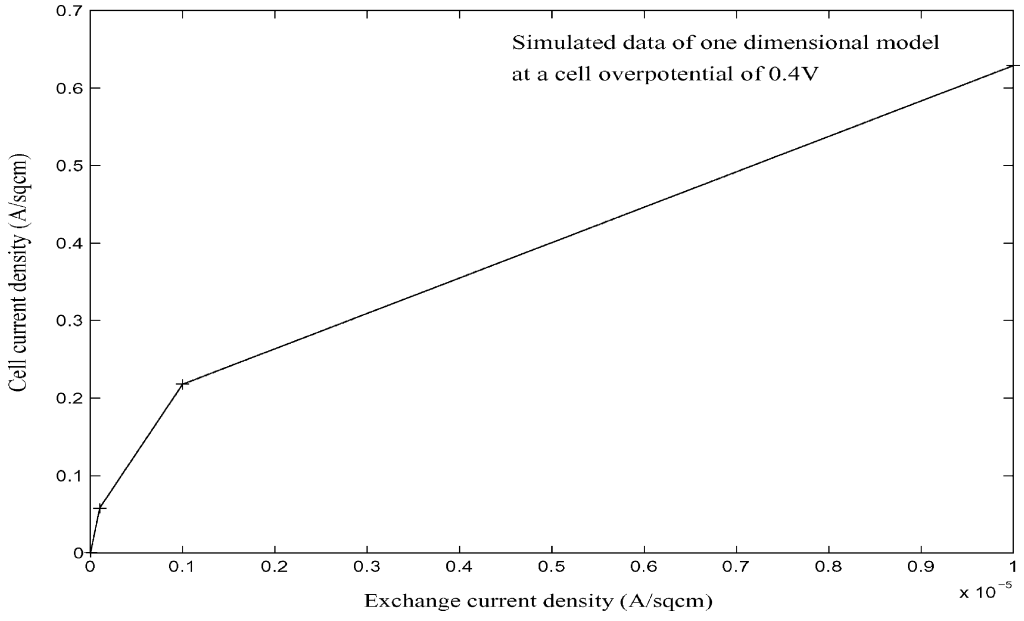

Fig. 16. Effect of exchange current density on electrode performance.

with acid drying. With the help of the model the water loss can be predicted and humidification of hydrogen gas can be done accordingly.

5. Conclusions

The model developed helps in analyzing the distribution pattern of oxygen partial pressure at various points of a composite porous gas diffusion cathode of a PAFC. Current generation at various points of a PAFC cathode depends upon local oxygen concentration. This model helps in determining the area(s) of low oxygen concentration and, thus, is helpful for designing various components of PAFC stacks. The model has been extensively used in NMRL for designing of groove pattern for the oxygen flow field in graphite manifold plates and the optimum catalyst coating thickness.

References

[1] L. Perry Mike, J. Newman, J.E. Cairns, J. Electrochem. Soc. 145 (1) (1998) 5.
[2] A.J. Appelby, F.R. Foulkes, Fuel Cell Handbook, Van Nostrand, New York, 1989.
[3] R.R. Barthelemy, Defense Applications of Fuel Cells—Fuel Cells Technology Status and Applications, Institute of Gas Technology, Chicago, IL, 1981.
[4] H. Celikar, M.A. Al-saleh, S. Gultekin, A.S. Al zakri, J. Electrochem. Soc. 138 (6) (1991) 1671.
[5] J. Giner, C. Hunter, J. Electrochem. Soc. 116 (8) (1969) 1124.
[6] J. Cutlip, S.C. Yang, Electrochim. Acta 36 (3/4) (1997) 547.
[7] R.J. Boersma, N.M. Sammes, J. Power Sources 66 (1997) 41.
[8] A.A. Kulikovsky, J. Divisek, A.A. Kornyshev, J. Electrochem. Soc. 146 (11) (1999) 3981.
[9] A Dutta, S. Shimpalee, J.W. Van Zee, J. Appl. Electrochem. 30 (2000) 135.
[10] G.J.M. Janssen, J. Electrochem. Soc. 148 (12) (2001) A1313.
[11] Y. Bultel, P. Ozil, R. Durand, J. Appl. Electrochem. 28 (1998) 269.
[12] K. Dannenberg, P. Ekdunge, G. Lindbergh, J. Appl. Electrochem. 30 (2000) 1377.
[13] J.S. Yi, T.V. Nguyen, J. Electrochem. Soc. 146 (1) (1999) 38.
[14] S. Um, C.Y. Wang, K.S. Chen, J. Electrochem. Soc. 147 (12) (2000) 4485.
[15] D. Natrajan, T.V. Nguyen, J. Electrochem. 148 (12) (2001) A1324.
[16] A.A. Kulikovsky, J. Appl. Electrochem. 30 (2000) 1005.
[17] A.A. Kulikovsky, J. Divisek, A.A. Kornyshev, J. Appl. Electrochem. 147 (3) (2000) 953.
[18] P. Argyropoulos, K. Scott, W.M. Taama, J. Appl. Electrochem. 30 (2000) 899.
[19] E. Fontes, C. Kagergren, G. Lindbergh, D. Simonsson, J. Appl. Electrochem. 27 (1997) 1149.
[20] F. Yoshida, N. One, Y. Izaka, T. Watanabe, T. Abe, J. Power Sources 70 (1998) 328.
[21] J.D. Fehribach, J.A. Prins-Jansen, K. Hemmes, J.H.W.D. Wit, F.W. Call, J. Appl. Electrochem. 30 (2000) 1015.
[22] R.B. Bird, W.E. Stewart, E.N. Lightfoot, Transport Pehnomena, Wiley, Newyork, 1960.
[23] D.T. Chin, H.H. Chang, J. Appl. Electrochem. 19 (1989) 95.
[24] Kirk and Othmer, Encyclopedia of Chemical Technology, Vol. 18, Wiley, 1991.
[25] W. Lenhert, J. Meusinger, F. Thom, J. Power Sources 87 (2000) 57.
[26] D. Bevers, K. Wohr, M. Yasuda, K. Oguru, J. Appl. Electrochem. 27 (1997) 1254.